Electronic Supplementary Information

Towards frustration in Eu(II) Archimedean tessellations

Hua Chen, Anna S. Manvell, Mariusz Kubus, Maja A. Dunstan, Giulia Lorusso, David Gracia, Mike S. B. Jørgensen, Søren Kegnæs, Fabrice Wilhelm, Andrei Rogalev, Marco Evangelisti, Kasper S. Pedersen

Chemical Communications

Synthesis

All procedures were carried out in an InertLab glovebox under a dry Ar atmosphere with an O_2 level <0.1 ppm and H_2O level <0.5 ppm. Elemental analysis was performed by the Mikroanalytisches Laboratorium Kolbe (Oberhausen, Germany). EuI_2 (99.99%), pyrazine (>99%), and 4,4′-bipyridine (98%) were supplied by Sigma-Aldrich and were used as received. Dry and oxygen-free solvents were obtained from a Puresolv MD 7 solvent purification system.

Synthesis of $EuI_2(pyz)_{5/2}$: A solution of EuI_2 (100 mg, 0.25 mmol) in acetonitrile (4 mL) was added to a solution of pyz (500 mg, 6.25 mmol) in acetonitrile (4 mL) and mixed with stirring for 1 h at room temperature. The solid material was isolated by vacuum filtration and dried under vacuum, yielding an orange microcrystalline powder (38.3 mg, 25%). Crystals suitable for X-ray diffraction were obtained via slow diffusion. A solution of EuI_2 (100 mg, 0.25 mmol) in acetonitrile (4 mL) was placed in a standard test tube (160 mm × 16 mm, soda glass). An acetonitrile solution (8 mL) of pyz (800 mg, 10 mmol) was slowly layered on top and the reaction mixture was left undisturbed at –20°C for 11 days. Anal. calcd. (found) for $C_{10}H_{10}I_2N_5Eu$: 19.8 (19.9); H, 1.66 (1.67); N, 11.6 (11.5); I, 41.9 (41.5); Eu, 25.1 (24.8).

Synthesis of $EuI_2(bipy)_{5/2}$: The method is similar to that of **$EuI_2(pyz)_{2.5}$**. A solution of EuI_2 (101.3 mg, 0.250 mmol) in acetonitrile (3.5 mL) and bipy (195 mg, 1.25 mmol) in acetonitrile (3.5 mL) were mixed and stirred for 2 h at room temperature. The precipitate was isolated by vacuum filtration, yielding an orange microcrystalline powder (134.6 mg, 64%). Single crystals suitable for X-ray diffraction were obtained via slow diffusion. EuI_2 (10.1 mg, 0.025 mmol) in acetonitrile (2 mL) was placed in an NMR tube (tube diameter 5 mm, size 7 in.). A solution of bipy (19.5 mg, 0.125 mmol) in acetonitrile (2 mL) was carefully layered on top and the reaction mixture was left undisturbed at –20°C for 14 days. Anal. calcd. (found) for $C_{10}H_{10}I_2N_5Eu$ (corresponding to $EuI_2(bipy)_{2.5}{\cdot}CH_3CN$): C, 38.7 (38.4); H, 2.75 (2.65); N, 10.0 (9.92); I, 30.4 (30.1); Eu, 18.2 (18.0).

Crystallography

Single crystals of **$EuI_2(pyz)_{2.5}$** and **$EuI_2(bipy)_{2.5}$** were covered in polybutene oil (Aldrich, >90%) under inert atmosphere. The single crystals were subsequently mounted on a nylon loop and measured on a SuperNova Dual Source CCD-diffractometer. The data were obtained at T = 120 K using Cu Kα (λ = 1.5406 Å; **$EuI_2(pyz)_{5/2}$**) or Mo Kα (λ = 0.71073 Å; **$EuI_2(bipy)_{5/2}$**) radiation. An absorption correction was applied to the data using a numerical absorption correction based on gaussian integration over a multifaceted crystal model in CrysAlisPro. The structures were solved by using the olex2.solve[1] structure solution program in Olex2[2] and refined by least squares minimization on F^2 using SHELXL.[3] All non-hydrogen atoms were refined anisotropically. Hydrogen atoms were placed using a riding model and refined isotropically. The data for **$EuI_2(pyz)_{5/2}$** were refined using a solvent mask, for which 35 electrons were found in a volume of 208 Å^3 in 1 void per unit cell. This is consistent with the presence of 0.75 CH_3CN per formula unit which accounts for 33 electrons per unit cell. For **$EuI_2(bipy)_{5/2}$**, a solvent mask was also calculated and 70 electrons were found in a volume of 315 Å^3 in 1 void per unit cell. This is consistent with the presence of 1.5 CH_3CN per formula unit which account for 66 electrons per unit cell. For **$EuI_2(bipy)_{2.5}$**, the atoms of the modelled acetonitrile solvent of crystallization were restrained to have similar anisotropic displacement parameters. One of the bipy ligands was also modelled with the atoms restrained to have similar anisotropic displacement parameters with rigid bond restraints. Elemental analysis and magnetometry obtained on both compounds are consistent with loss of the disordered acetonitrile solvent in the bulk samples. The crystallographic information has been deposited in the Cambridge Crystallographic Data Centre under the accession codes CCDC 2219223 (**$EuI_2(pyz)_{5/2}$**) and 2219222 (**$EuI_2(bipy)_{5/2}$**).

The powder X-ray diffraction of **$EuI_2(pyz)_{2.5}$** and **$EuI_2(bipy)_{2.5}$** was measured at room temperature, restrained in tape sealed under inert atmosphere, with a Huber G670 powder diffractometer using Cu Kα (λ = 1.5406 Å, quartz monochromator) radiation in transmission mode. The data for **$EuI_2(pyz)_{2.5}$** and **$EuI_2(bipy)_{2.5}$** were obtained with exposure times of 10 mins and 60 mins, respectively. The Rietveld method was used to confirm phase purity and to determine the unit cell parameters at room temperature. The analysis was performed in the HighScore Plus 5.1.0 program suite.[4] All atomic positions and occupancies were kept fixed during the refinement process and the refinements were performed with a correction for preferred orientation. A good fit between the observed and calculated patterns for **$EuI_2(pyz)_{5/2}$** (R_{wp} = 4.06%) and **$EuI_2(bipy)_{5/2}$** (R_{wp} = 3.03%) confirms the sample purity of both compounds. Small additional reflections and discrepancies between observed and calculated patterns are probably a result of minor impurities present in the samples, materials

crystallinity, and partial decomposition due to high reactivity. The refined room-temperature lattice parameters (Å, °) for **$EuI_2(pyz)_{5/2}$** were a = 8.21(3), b = 9.02(3), c = 12.66(4), α = 93.159(3), β = 96.131(6), γ = 92.379(2) and for **$EuI_2(bipy)_{5/2}$**: a = 9.22(3), b = 10.03(4), c = 19.16(7), α = 83.778(9), β = 81.64(1), γ = 79.46(1).

X-ray spectroscopy

X-ray absorption (XANES) and dichroism (XMCD) spectra at the Eu $L_{2,3}$-edges were obtained at the ID12 beamline of the ESRF – The European Synchrotron Facility in Grenoble, France, which is dedicated to polarization dependent X-ray spectroscopy at 2–15 keV incident photon energies.[5] The circularly polarized photon beam was generated by a HELIOS-II type undulator and monochromatized by a Si <111> double-crystal monochromator. The low-temperature XANES and XMCD spectra of **$EuI_2(pyz)_{5/2}$** were obtained using the total fluorescence yield detection mode, while the room-temperature XANES spectra of **$EuI_2(pyz)_{5/2}$** and EuI_2, were obtained in transmission geometry. The former were corrected for re-absorption effects.

The XMCD spectra were systematically obtained in both field directions to exclude the risk of experimental artefacts. The isotropic spectra were obtained as the sum of spectra with right and left circularly polarized X-rays and were normalized to zero before the absorption edge and to unity above the edge. The L_2 spectral intensities were divided by 2 reflecting the occupation ratios of the $2p_{3/2}$ and $2p_{1/2}$ core states. The sample temperature of T = 6 K was determined by scaling the magnetic field and temperature dependent XMCD signal intensity to the M versus $\mu_0 HT^{-1}$ data obtained from bulk magnetometry.

Magnetization measurements and analysis and heat capacity measurements and analysis

The direct-current (dc) magnetization measurements were performed with the vibrating sample magnetometer (VSM) option using a QuantumDesign Dynacool Physical Property Measurement System (PPMS) in the temperature range from 2 K to 270 K and in magnetic fields between $\mu_0 H$ = ±9 T. Polycrystalline samples were loaded and sealed in standard QuantumDesign powder capsules and sealed with Teflon tape inside an Ar-filled glovebox. The magnetization data were corrected for diamagnetic contributions of both the sample and the sample container. Alternating current (ac) susceptibility measurements on **$EuI_2(pyz)_{5/2}$** were performed on the same instrument by using the ACMS-II option. The polycrystalline sample was loaded and sealed in a polycarbonate capsule which was subsequently immobilized in a drinking straw. The data were acquired between 1.8 K and 20 K using ac frequencies from 10 Hz to 10 kHz. The model calculations of the dc magnetization data were

performed using the MagProp programme which is included in the DAVE programme suite.[6] The calculations utilized matrix-diagonalization of the spin-Hamiltonian matrix and were based on the isotropic Zeeman Hamiltonian $\hat{\mathscr{H}} = g\mu_B\mu_0 H\hat{S}$.

The heat capacity, C_p, was measured by the relaxation method at constant magnetic fields from 0 to 7 T, using a QuantumDesign PPMS, equipped with a ^{3}He option. The sample, in the form of a microcrystalline powder, was mixed with Apiezon N thermal grease inside an Ar filled glovebox. The magnetic field was applied parallel to the platform of the calorimeter to minimize overheating by eddy currents in the measuring system. The magnetocaloric effect (MCE) in the form of the magnetic entropy change, $-\Delta S_m$, is straightforwardly obtained from the entropy data. From $C_p(T,\mu_0 H)$, we calculate the entropy $S(T,\mu_0 H)$, according to $S = \int C_p/T \, dT$. Figure S13 shows the temperature-dependence of the entropy for several applied field values. At high temperatures, $S(T,\mu_0 H)$ becomes field-independent and increases because of the lattice contribution. At the lowest temperatures, $S(T,\mu_0 H)$ is dominated by the magnetic contribution and, for $\mu_0 H$ = 0 T, the entropy approaches the maximum magnetic entropy value per mol involved, corresponding to $R \ln(2S_{Eu}+1) = 2.08\ R$ for $S_{Eu} = 7/2$.

DFT Calculations

The DFT calculations were performed using the ORCA programme suite,[7] employing scalar relativistic effects through the 0th-order regular approximation (ZORA).[8] The experimentally determined atomic coordinates of **$EuI_2(pyz)_{5/2}$** and **$EuI_2(bipy)_{5/2}$** were used to generated dieuropium fragments as input without any subsequent geometry optimization. For all calculations, the B3LYP functional was combined with the scalar-relativistically recontracted (SARC) version of the ZORA-def2-TZVP basis set[9] together with the corresponding auxiliary basis.[10] For both systems a high-spin (HS) S = 7 calculation and a $S_{Eu1} = 7/2 - S_{Eu2} = 7/2$ broken symmetry calculation (BS(7,7)) were performed. The calculated energy difference between the BS and HS states were utilized to evaluate the superexchange coupling constant, J, obtained as suggested by Yamaguchi.[11] Spin density plots and Kohn-Sham frontier orbital plots were rendered using the VMD program.[12]

Table S1. Crystal data for compounds **$EuI_2(pyz)_{5/2}$** and **$EuI_2(bipy)_{5/2}$**.

Compound	**$EuI_2(pyz)_{5/2}$**	**$EuI_2(bipy)_{5/2}$**
CCDC deposition number	2219223	2219222
Temperature / K	120	120
Crystal system	Triclinic	Triclinic
Space group	$P\bar{1}$	$P\bar{1}$
a / Å	8.1924(6)	9.0699(3)
b / Å	8.9731(8)	10.0551(4)
c / Å	12.6268(11)	19.0931(8)
α / °	93.079(7)	88.744(3)
β / °	95.703(6)	82.778(3)
γ / °	92.678(7)	79.924(3)
Volume / Å^3	921.02(13)	1700.81(11)
Z	2	2
Crystal dimensions / mm	0.135 × 0.114 × 0.092	0.234 × 0.104 × 0.072
ρ_{calc} / g cm^{-1}	2.185	1.635
Radiation	Cu Kα (λ = 1.54184 Å)	Mo Kα (λ = 0.71073 Å)
2θ range for data collection / °	7.048 to 153.024	6.674 to 59.356
Index ranges	$-7 \le h \le 10$ $-11 \le k \le 11$ $-14 \le l \le 15$	$-12 \le h \le 12$ $-13 \le k \le 13$ $-25 \le l \le 26$
Reflections collected	7745	37841
Independent reflections	3809 [R_{int} = 0.0531]	8644 [R_{int} = 0.0384]
Data/restraints/parameters	3809/0/163	8644/48/314
Goodness-of-fit on F^2	1.054	1.046
Final R_1 index of [$F^2 \ge 2\sigma(F^2)$]	0.0490	0.0427
Final wR_1 index of [F^2]	0.0637	0.0558
Largest diff. peak/hole/ e Å^{-3}	1.98/–1.26	1.59/–1.67

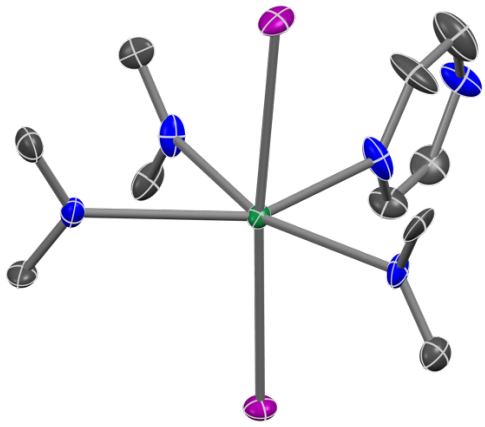

Figure S1. Thermal ellipsoid (50% probability level) plot of the asymmetric unit of **$EuI_2(pyz)_{5/2}$**. Colour code: Eu, green; I, purple; N, blue; C, grey. Hydrogen atoms have been omitted.

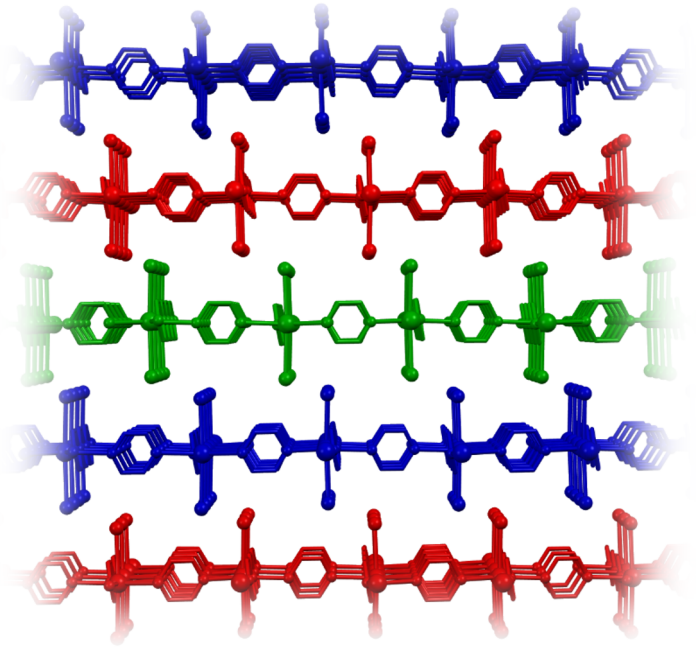

Figure S2. Perspective view of the layered structure in **$EuI_2(pyz)_{5/2}$**. Hydrogen atoms have been omitted. The layers are coloured to highlight the ABC type packing.

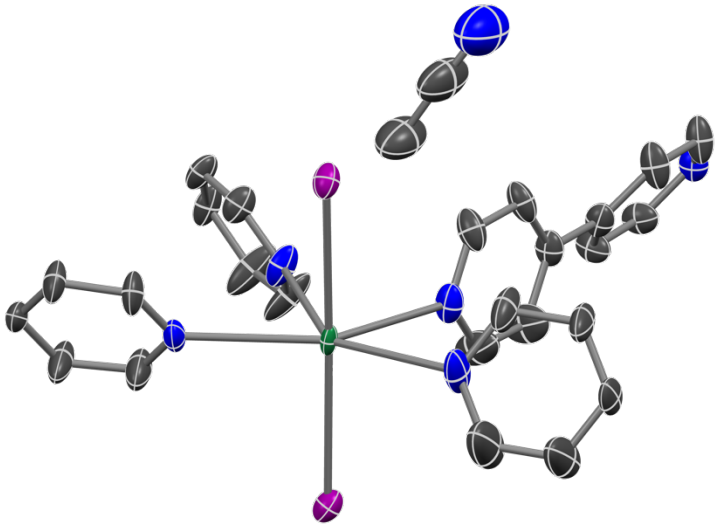

Figure S3. Thermal ellipsoid (50% probability level) plot of the asymmetric unit of **$EuI_2(bipy)_{5/2}$**. Colour code: Eu, green; I, purple; N, blue; C, grey. Hydrogen atoms have been omitted.

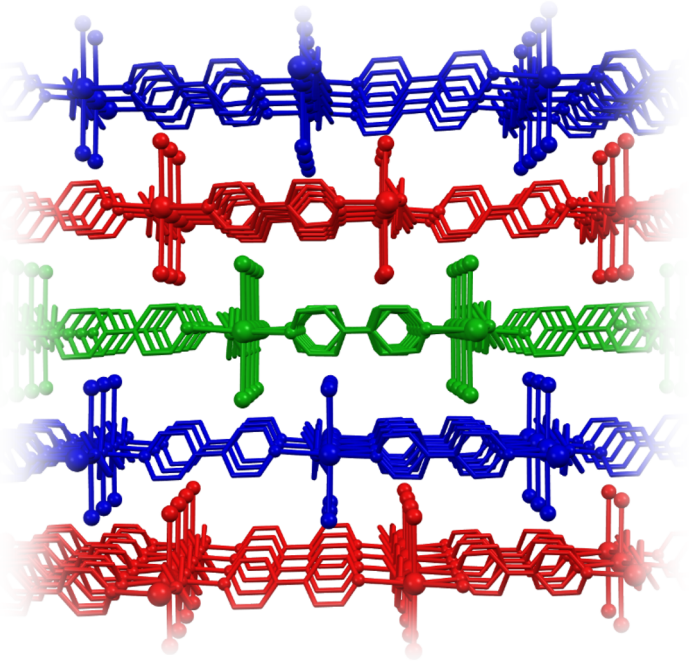

Figure S4. Perspective view of the layered structure in **$EuI_2(bipy)_{5/2}$**. Hydrogen atoms and MeCN have been omitted. The layers are coloured to highlight the ABC type packing.

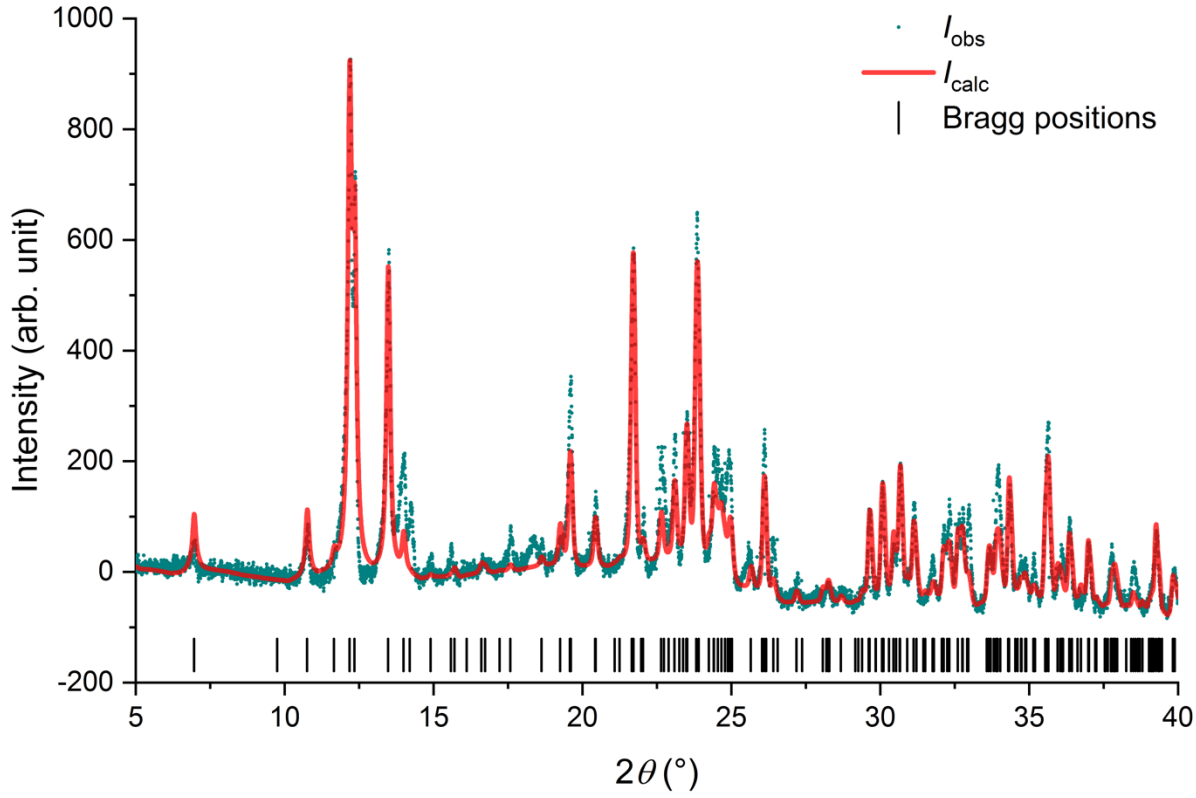

Figure S5. Powder X-ray diffractogram of **$EuI_2(pyz)_{5/2}$** recorded at room temperature (turquoise trace) and the Rietveld fit (red trace).

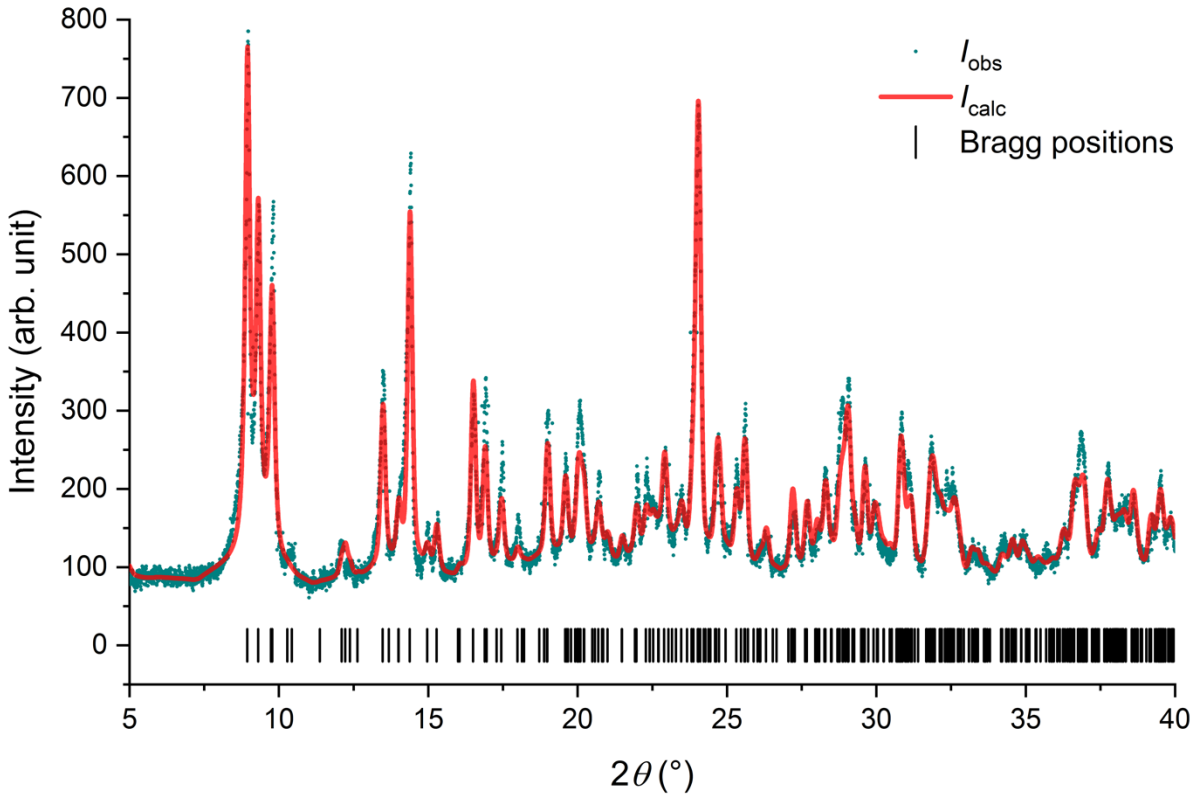

Figure S6. Powder X-ray diffractogram of **$EuI_2(bipy)_{5/2}$** recorded at room temperature (turquoise trace) and the Rietveld fit (red trace).

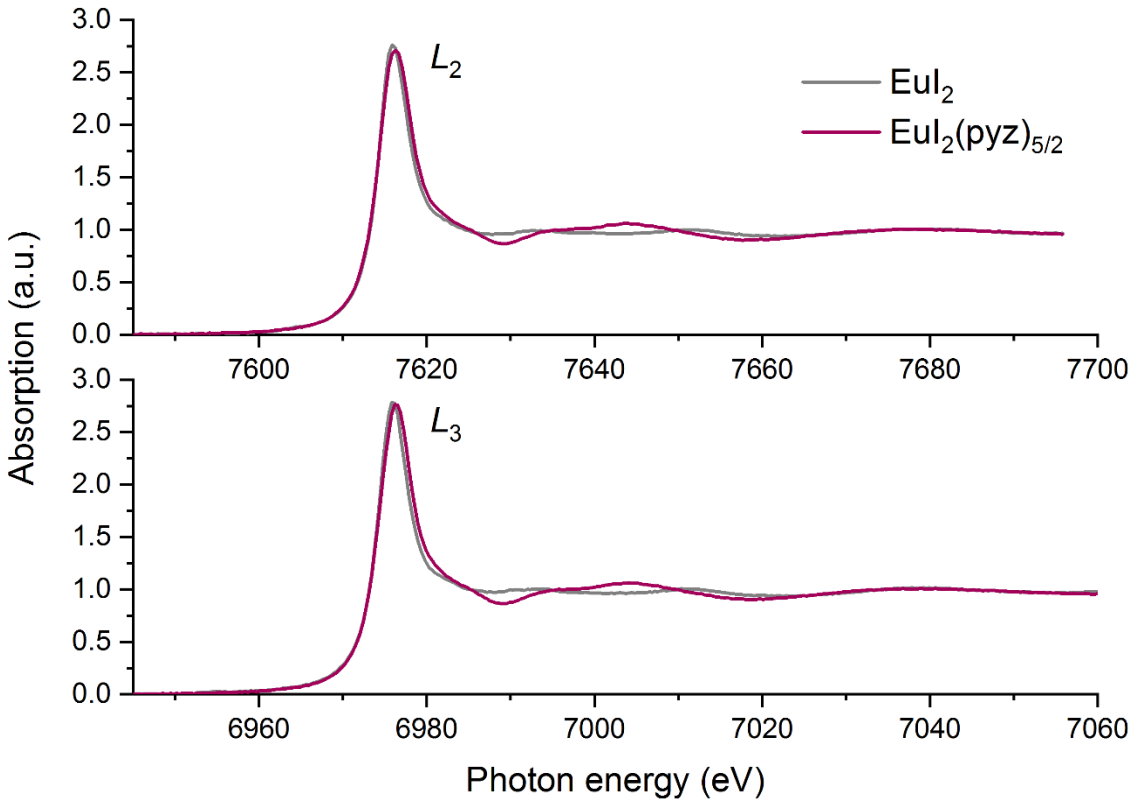

Figure S7. Room-temperature XANES spectra of **$EuI_2(pyz)_{5/2}$** together with a EuI_2 reference at the Eu $L_{2,3}$ edges.

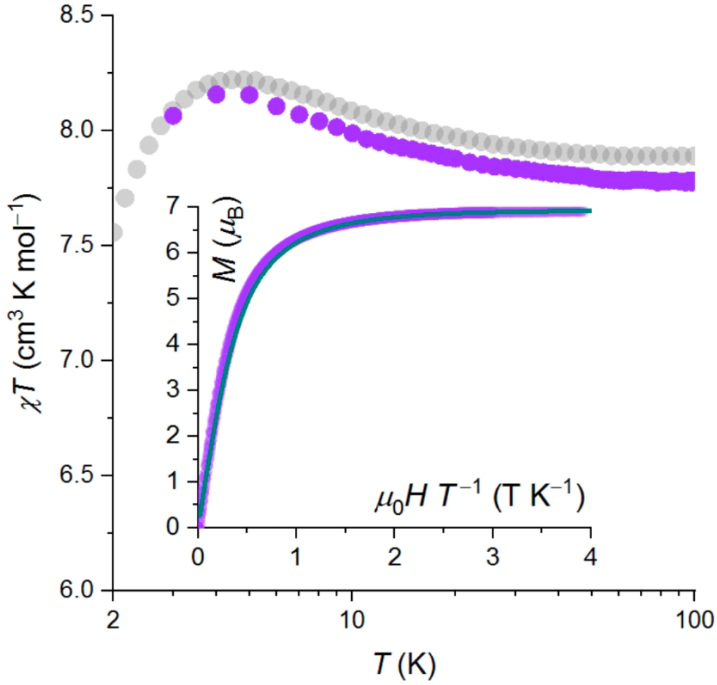

Figure S8. Temperature dependence of the χT ($\mu_0 H$ = 0.1 T) product for **$EuI_2(bipy)_{5/2}$**. The grey trace shows the data for **$EuI_2(pyz)_{5/2}$**. Inset: Field-dependence of the magnetization plotted against $\mu_0 H\ T^{-1}$. The solid, turquoise line represents the Brillouin function for S = 7/2 with g = 1.98.

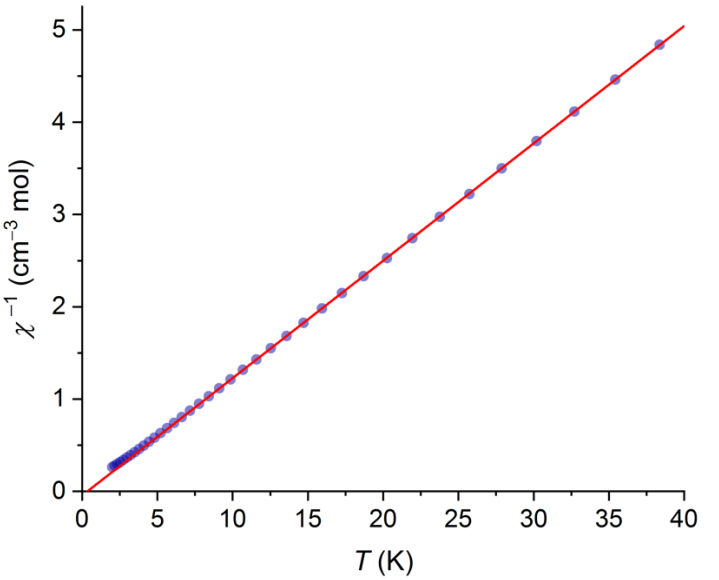

Figure S9. Inverse magnetic susceptibility ($\mu_0 H$ = 0.01 T) vs. temperature plot for **$EuI_2(pyz)_{5/2}$**. The solid red line is the fit to the Curie-Weiss law (10–40 K) as described in the main text.

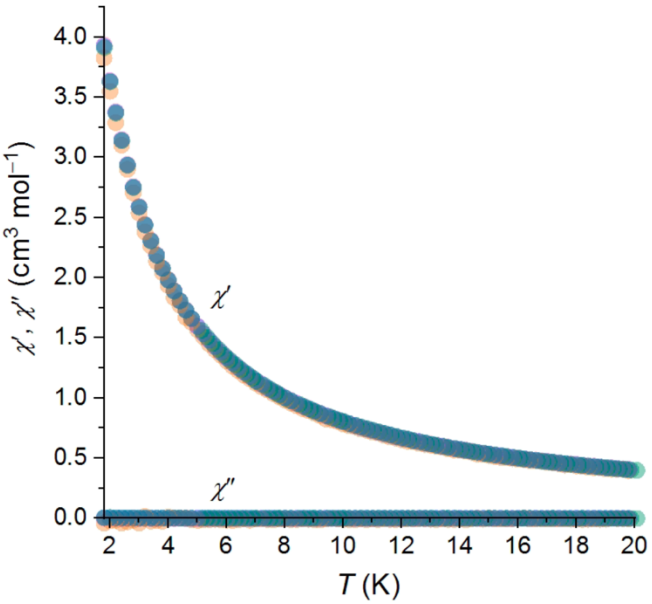

Figure S10. Temperature dependence of the in-phase (χ') and out-of-phase (χ'') component of the ac susceptibility for **$EuI_2(pyz)_{5/2}$** obtained with ac frequencies 10 Hz, 100 Hz, 1 kHz, and 10 kHz, and in the absence of a dc magnetic field.

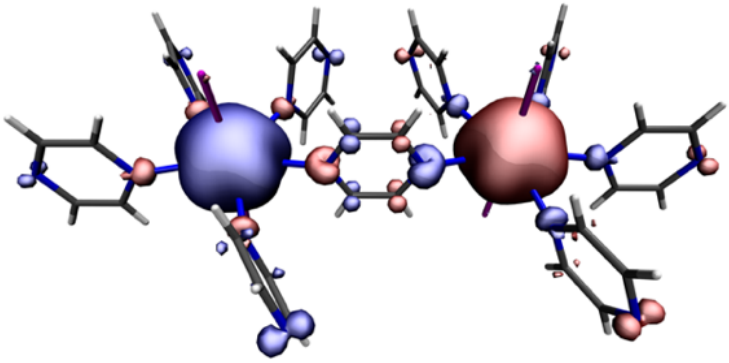

Figure S11. DFT-calculated spin density plot (isosurface value = ±0.001 a.u.) for the (7,7)-broken symmetry state of a dinuclear fragment of $EuI_2(pyz)_{5/2}$.

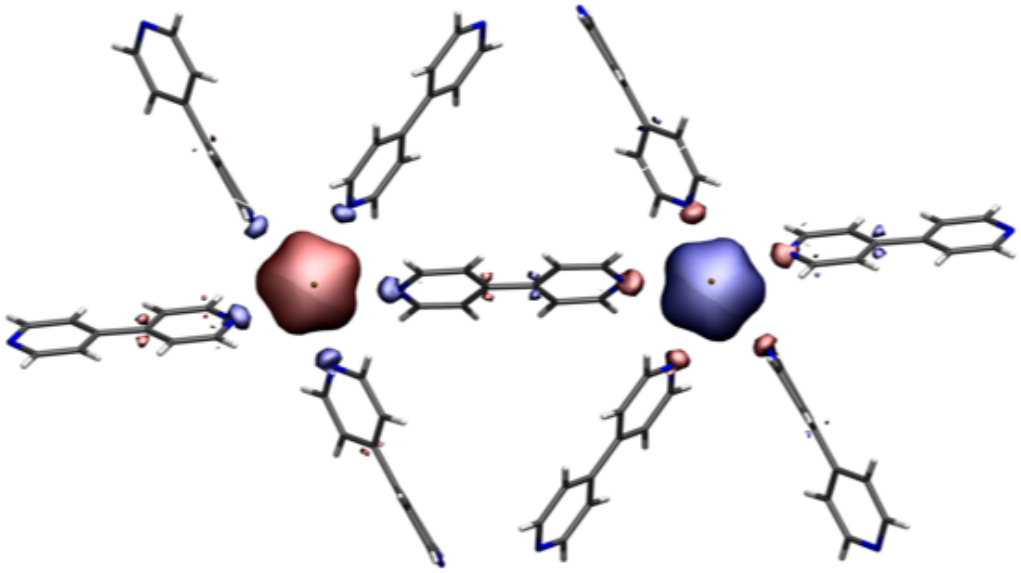

Figure S12. DFT-calculated spin density of the (7,7)-broken symmetry state of a $[Eu_2I_4(bipy)_9]$ fragment in **$EuI_2(bipy)_{5/2}$** plotted at an iso-surface value of ±0.001 a.u.

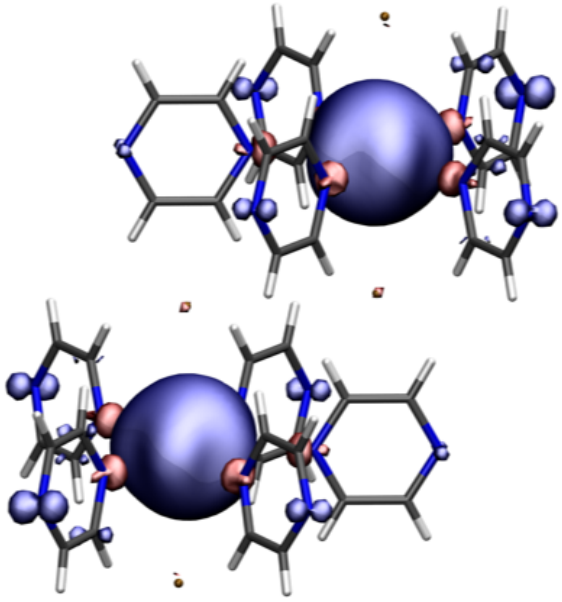

Figure S13. DFT-calculated spin density of the high-spin state of two adjacent $[EuI_2(pyz)_5]$ fragments in **$EuI_2(pyz)_{5/2}$** plotted at iso-surface value of ±0.001 a.u.

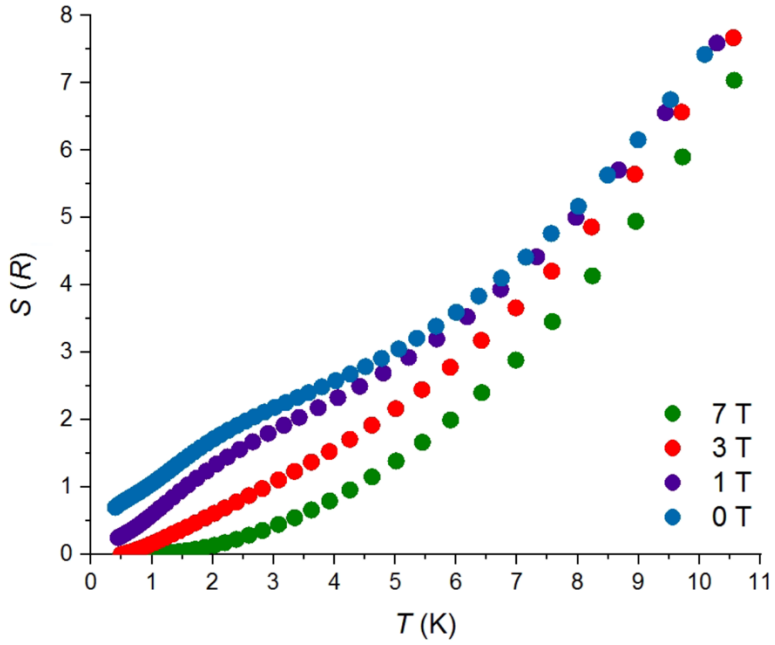

Figure S14. Low-temperature entropy data at selected magnetic fields for **$EuI_2(pyz)_{5/2}$** obtained from the specific heat as described above.

References

[1] L. J. Bourhis, O. V. Dolomanov, R. J. Gildea, J. A. K. Howard, H. Puschmann, *Acta Cryst.* **2015**, *A71*, 59.

[2] O. V. Dolomanov, L. J. Bourhis, R. J. Gildea, J. A. K. Howard, H. Puschmann, *J. Appl. Cryst.* **2009**, *42*, 339-341.

[3] G.M. Sheldrick, *Acta Cryst.* **2015**, *C71*, 3.

[4] T. Degen, M. Sadki, E. Bron, U. König, G. Nénert, The HighScore suite. *Powder Diffraction,* **2014**, *29* (S2), S13-S18.

[5] A. Rogalev, J. Goulon, C. Goulon-Ginet and C. Malgrange, Lecture Notes in Physics, edited by: E. Beaurepaire, F. Scheurer, G. Krill and J.-P. Kappler, 2001, Vol. 565, p. 60.

[6] R. T. Azuah, L. R. Kneller, Y. Qiu, P. L. W. Tregenna-Piggott, C. M. Brown, J. R. D. Copley, R. M. Dimeo, *J. Res. Natl. Inst. Stand. Technol.* **2009**, *114*, 341.

[7] F. Neese, *WIREs Comput. Mol. Sci.* **2018**, *8*, e1327

[8] (a) E. van Lenthe, E. J. Baerends, J. G. Snijders, *J. Chem. Phys.* **1993**, *99*, 4597; (b) C. J. van Wüllen, *J. Chem. Phys.* **1998**, *109*, 392.

[9] (a) D. A. Pantazis, F. Neese, *J. Chem. Theory Comput.* **2009**, *5*, 2229; (b) J. D. Rolfes, F. Neese, D. A. Pantazis, *J. Comput. Chem.* **2020**, *41*, 1842.

[10] (a) F. Weigend, *Phys. Chem. Chem. Phys*. **2006**, *8*, 1057; (b) D. A. Pantazis, F. Neese, *J. Chem. Theory Comput.* **2009**, *5*, 2229; (c) D. A. Pantazis, X. Y. Chen, C. R. Landis, F. Neese, *J. Chem. Theory Comput.* **2008**, *4*, 908; (d) D. A. Pantazis, F. Neese, *Theor. Chem. Acc.* **2012**, *131*, 1292; (e) D. A. Pantazis, F. Neese, *J. Chem. Theory Comput*. **2011**, *7*, 677.

[11] (a) K. Yamaguchi, Y. Takahara, T. Fueno, in *Applied Quantum Chemistry*; V. H. Smith, H. F. Schaefer, K. Morokuma, Eds.; D. Reidel: Boston, **1986**; p. 155; (b) S. Yamanaka, T. Kawakami, H. Nagao, K. Yamaguchi, *Chem. Phys. Lett.* **1994**, *231*, 25.

[12] (a) W. Humphrey, A. Dalke, K. Schulten, *J. Molec. Graphics* **1996**, 14, 33; (b) Website: http://www.ks.uiuc.eu/Researcg/vmd